Vacation Work 25th of June to 3rd of August

Calvin Tock

Part I

Transmittance through an Aerosol Cell

Introduction When modeling transmission of light through an aerosol cell, a simple model looks only at the direct beam and ignores multiple scattering. This model gives the transmittance as $e^{-\tau}$ (Direct beam transmittance), where τ is the Aerosol Optical Depth. An investigation into the strength of this model in light of additional factors was conducted.

Definitions Some useful definitions for terms in this report are provided here.

- Transmittance - the fraction of incident light of a given wavelength which passes through the cell.
- (Aerosol) Optical Depth (AOD) - A measure of transparency, defined mathematically as $-log_e$(Direct beam Transmittance).
- Single Scatter Albedo - A fraction which provides the probability of a single photon's interaction with an aerosol particle resulting in scattering rather than absorption. It has values between 0 (certain absorption) and 1 (certain scattering).
- Multiple Scattering - Scattering where a photon interacts with the aerosol multiple times before being detected.
- IDL - Interactive Data Language. This is the software used to produce the graphs in this report.
- DISORT - A FORTRAN programme (which can be called in IDL) which calculates multiple scattering, amongst other things.
- Acceptance angle - The angle for which photons can be detected leaving the aerosol cell.
- Asymmetry factor - This parameterises the angular distribution of scattering from a particle. A value of 0 means isotropic scattering, 1 means the light is scattered entirely forward, and -1 means the light is scattered entirely backwards. Using this parameter is in fact an approximation, and the angular distribution can be better calculated using Legendre Polynomials.
- Extinction coefficient β^{ext} - a path-dependent measure of how a size distribution of particles cause extinction for a light beam. AOD can be defined as the integral of the extinction coefficient along the path of the beam. The beam length used in this report was 0.25 meters.
- Size parameter x - A parameter often used instead of radius. $x = 2\pi r/\lambda$.
- Aspect ratio AR- for ellipsoids generated by rotating an ellipse around one of its

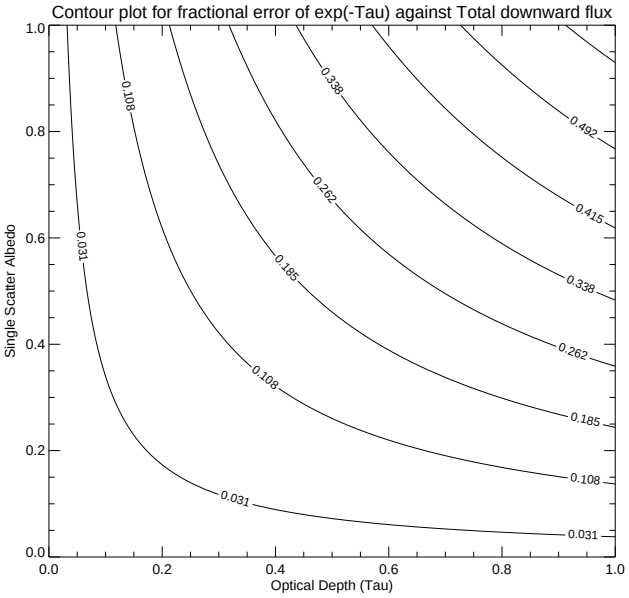

Figure 1: Contour plot of Fractional error between the Total transmittance and the direct-beam-only transmittance at a fixed asymmetry factor, g (=0.75), and varying AODs and Albedos.

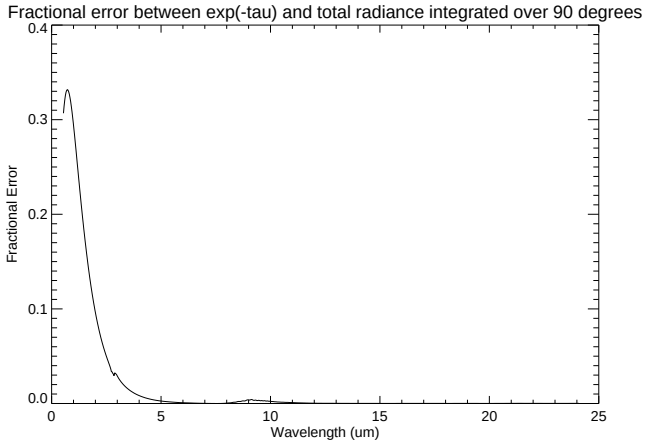

Figure 2: Fractional Error between $e^{-\tau}$ and total transmittance, calculated using Mie scattering, and integrated over the whole 2π solid angle. (Acceptance angle = $\pi/2$).

axes, their non-sphericity can be described by the ratio of the axis perpendicular to the rotation divided by the rotation axis. This is called the aspect ratio in this report.

Multiple scattering for spherical particles An IDL code was written so that the fractional error between $e^{-\tau}$ and the transmittance calculated by DISORT (which includes light from the direct beam and diffuse light leaving the cell at any acceptance angle) could be plotted against varying Single scatter albedos and AODs as a contour plot. This can be seen in Figure 1.

It can be seen that multiple scattering has a significant effect on the transmittance through the aerosol cell, as errors of up to 50% can occur at certain optical depths and Albedos.

It was noted that albedo and optical depth are not unrelated, and that the scattering can be more accurately calculated using Mie scattering theory, when the lognormal distribution (parameterized by the number density, particle size and mean radius), wavenumber of light used, and the complex refractive index of the aerosol at the respective wavenumber are provided. Using the ASO Ash data provided [1], fractional error between $e^{-\tau}$ and total transmittance could be plotted against wavelength. (Figure 2).

The errors at low wavelengths here are as high as 30%. This could have been a significant problem, had it not been for the fact that the acceptance angle for the detector is around $\theta = 1^\circ$, and that most of the multiply scattered light is not detected. The IDL code was therefore edited to use this acceptance angle to more accurately calculate the transmittance. It was also noted that by replacing the approximation based on the asymmetry factor by the full Legendre calculation, more accurate results could be obtained. Transmittance for the case of reduced acceptance angle was plotted against wavelength, and the fractional error was again plotted. These can be seen in Figure 3, and it can be seen that this leads to a much smaller deviation from the simple model.

It was desirable to know for what number density the fractional error reached 1%, and also the transmittance at this N. This was calculated and plotted in Figure 4.

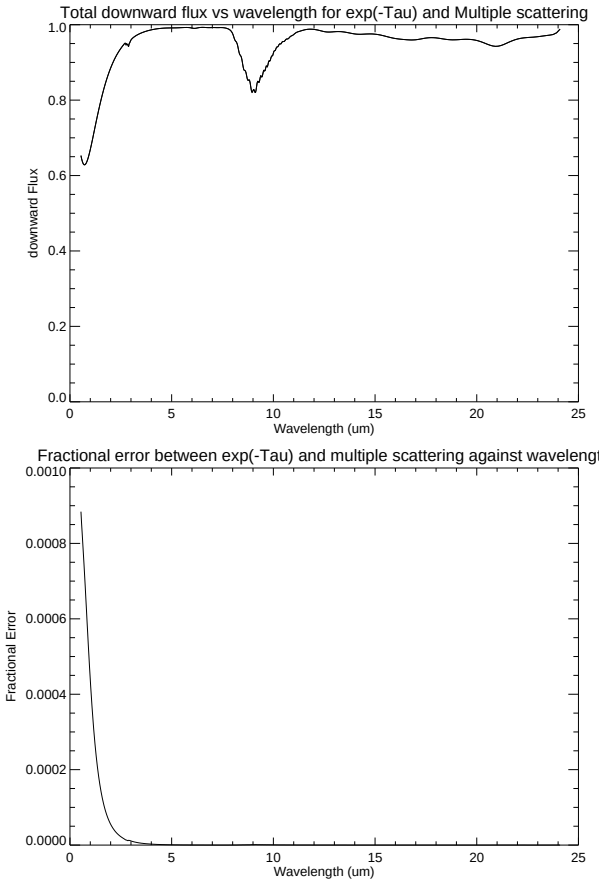

Figure 3: Top: Transmittance through the aerosol cell against wavelength for a 1°acceptance angle, N = 1x10^{6}cm^{-3} and mean radius = 0.37μm. Bottom: Fractional error between $e^{-\tau}$ and transmittance through the 1°acceptance angle against wavelength for the same parameters.

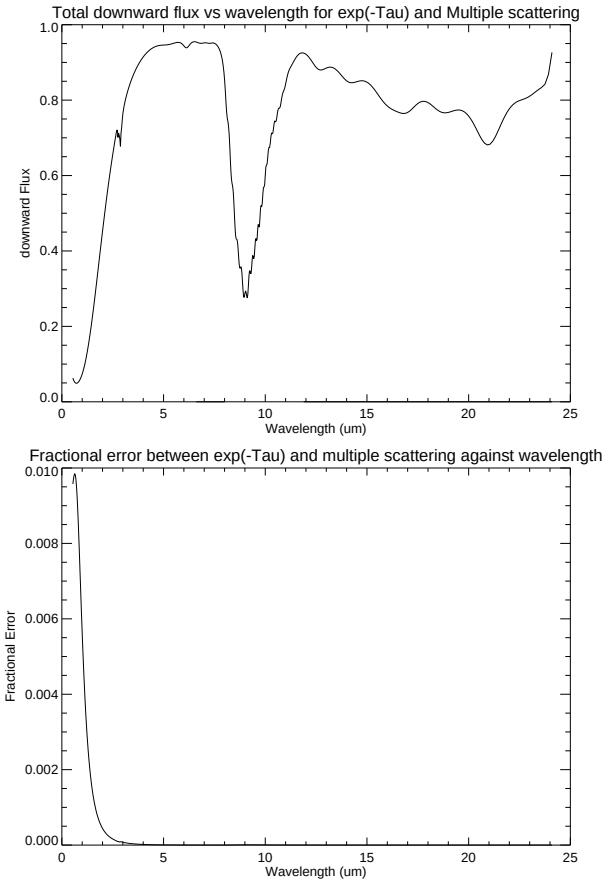

Figure 4: Top: Transmittance through the aerosol cell against wavelength for a 1°acceptance angle, N = 6.5x10^{6}cm^{-3} and mean radius = 0.37μm. Bottom: Fractional error between $e^{-\tau}$ and transmittance through the 1°acceptance angle against wavelength for the same parameters.

Non-spherical particles When non-spherical particles were considered, a modified version of the Mie scattering code was used [2] and the fractional error between transmittances for spherical and non-spherical particles was calculated. This was plotted for a variety of number densities and mean radii, and can be seen in Figure 5. As the Dubovik code (Non-Spherical particle code) relies on lookup tables to calculate the extinction coefficients (which in turn are used to calculate transmittances), only a small range of the original data could be calculated directly. At lower wavelengths, the imaginary part of the complex refractive index (k) of the ASO data lies below the minimum value on the lookup table(k < 0.0005). To retrieve the Dubovik scattering values within this range, it is necessary to determine the best way of generating the extinction parameters given these very small refractive indexes.

Two possible solutions could be to either extrapolate the extinction parameter with respect to k, or to choose the extinction parameter evaluated at the lowest possible valid imaginary component, and use that for any subsequent, smaller ks (flooring). To look at the merits of each method, graphs were plotted comparing the extinction coefficients generated by the Mie code, and the Dubovik code when the aspect ratio was set to 1.0 (spherical particles). These plots used a fixed (but characteristic) wavenumber and real component, and varied k. They can be seen in Figure 6.

For larger particles and number densities, the errors between the extrapolated/floored values and the Mie code were small (1.3%), however, for smaller particle with lower densities, there can be around a 40% error for flooring, and when extrapolating, the method fails entirely, as it predicts a negative extinction parameter, which is unphysical. This suggests that the best way to look at data outside of the range of the lookup table is to use the flooring method.

As the feature of interest is the non-sphericity of the particles, (rather than the errors introduced due to discrepancies between the Mie code and the Dubovik lookup tables), graphs were plotted to look at the effect of non-sphericity on the extinction coefficient over a range of real and imaginary refractive indexes using Dubovik code for both spherical and non-spherical particles. This allows the fractional errors introduced due to non-sphericity to be observed. These graphs were plotted for several size parameters ($x = 0.14$, 1.4, 7 and 14), each with similar results. The plot for $x = 7$ (which had the largest difference) can bee seen in Figure 7.

These plots show that for most complex refractive indexes, non-sphericity provides no more than 5% errors at this particle density.

Using the ASO Ash data [1] instead of the range of refractive indexes shows the effect of non-sphericity on transmittance at low wavelengths. Plots for the fractional errors in transmittance between spherical and non-spherical particles with aspect ratios of 1.00 and 1.44 for a range of number densities and mean radii can be seen in Figure 8.

These plots show that non-sphericity is only a major source of errors when number densities and particle sizes are large.

Conclusion For wavelengths greater than $5\mu m$, multiple scattering is not a significant factor, and $e^{-\tau}$ works as an approximation. For wavelengths less than $5\mu m$, multiple scattering provides a large source of errors, even when the acceptance angle is factored into the calculations. In this regime, Mie scatting can be used to calculate transmittances to a greater accuracy. Non-sphericity of the aerosol particles does have an effect on transmittance, but it is only really significant at large number densities and particle sizes.

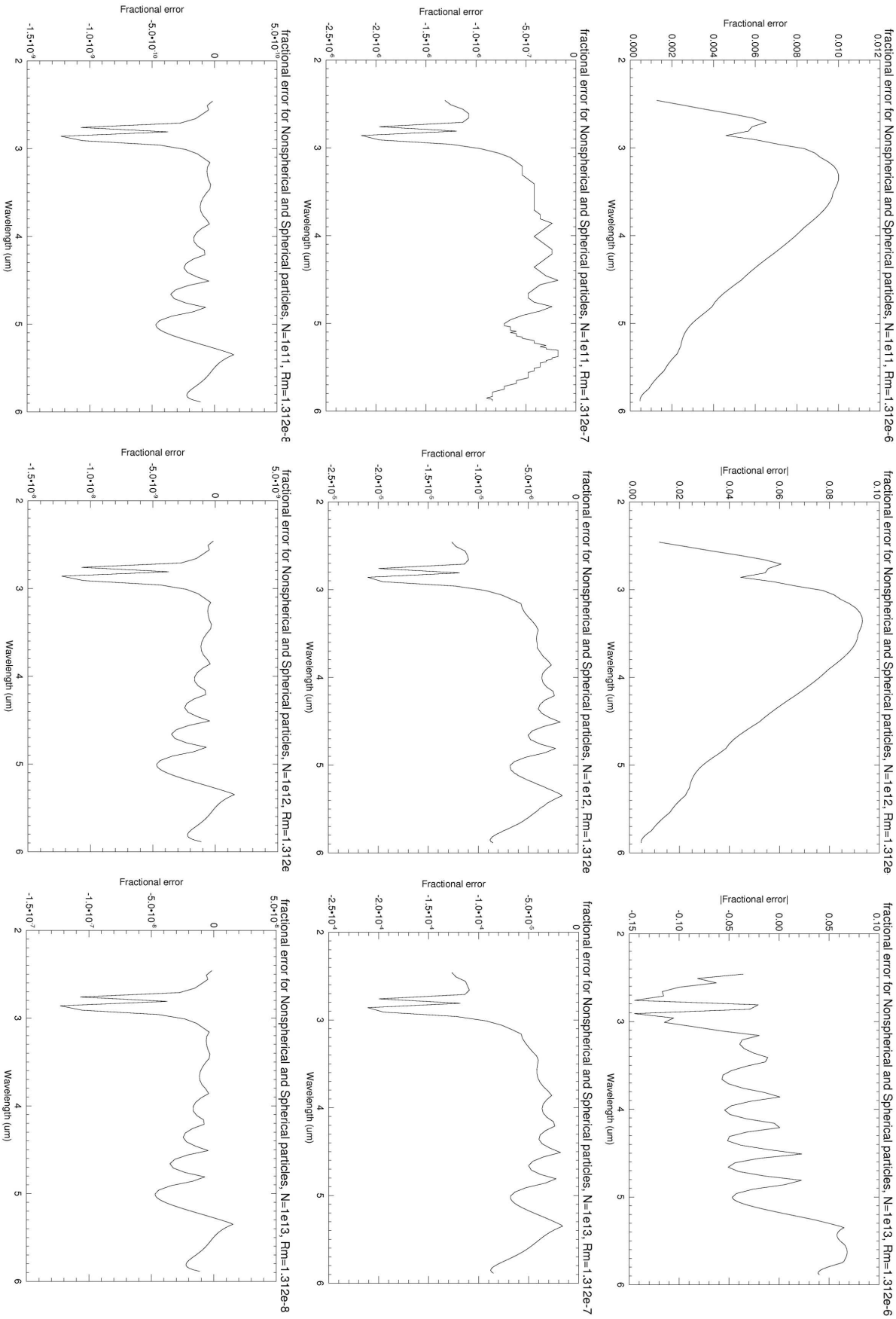

Figure 5: Plots of fractional error between Spherical and Non-Spherical scattering at various Number densities (N) and mean radii (Rm).

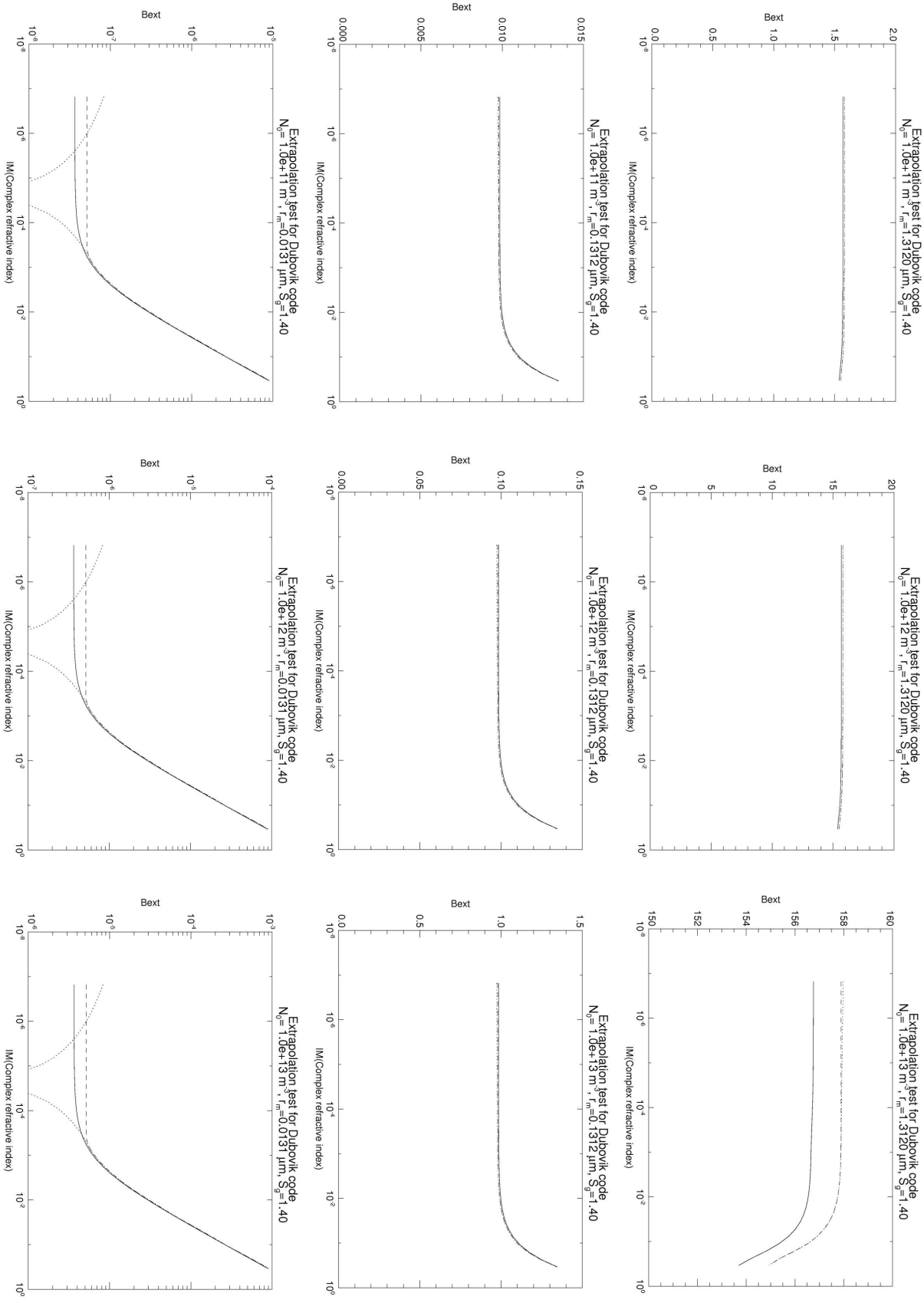

Figure 6: Plots of extinction coefficients against imaginary component of complex refractive index for spherical particles calculated using Mie code, and Dubovik code with two different types of extrapolation. Solid line = Mie code, Dashed line = Flooring, Dotted line = Extrapolation.

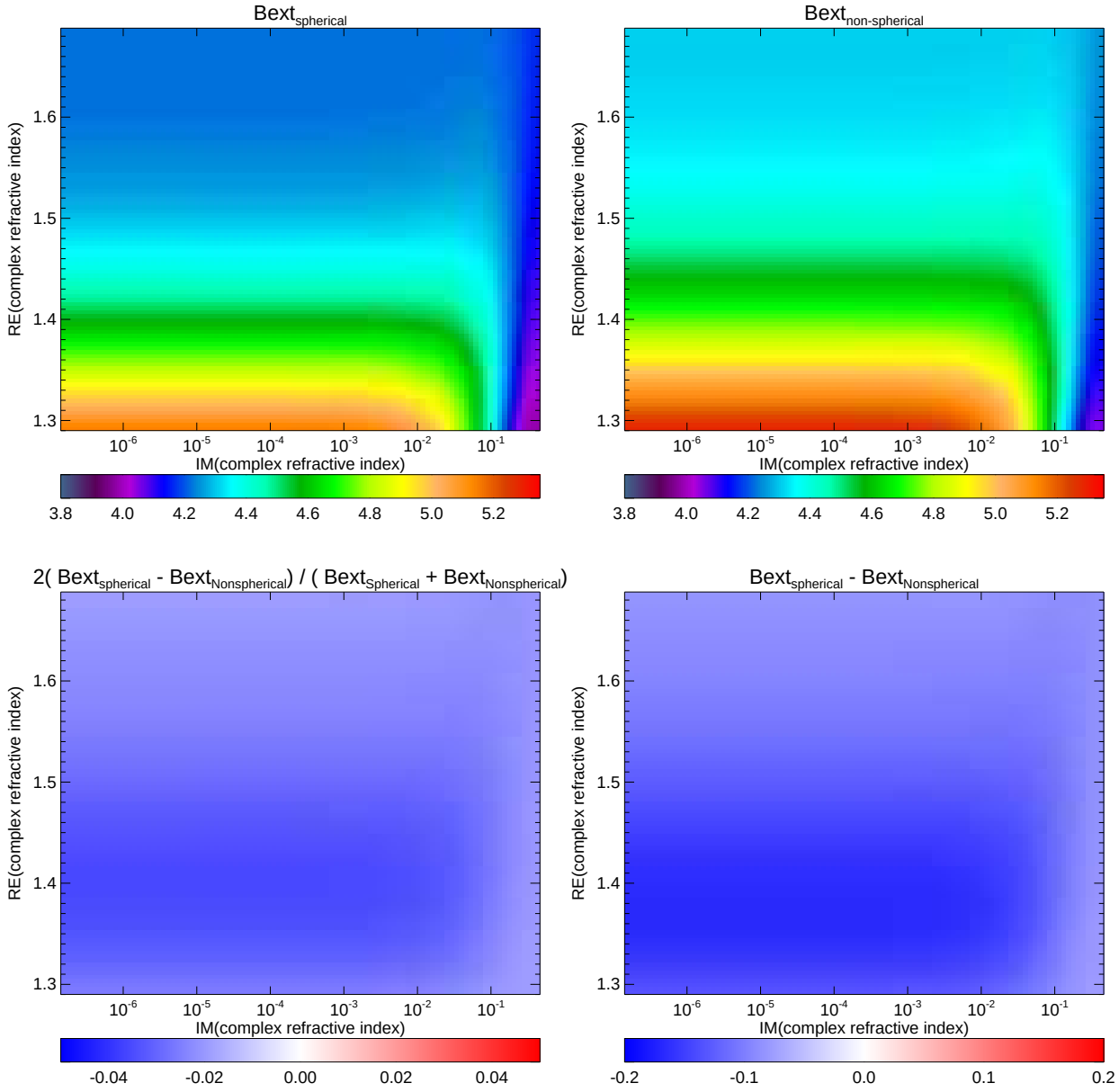

Figure 7: Top: Extinction coefficients calculated using Dubovik code for spherical (AR=1) and Non-spherical (AR=1.44) particles over a range of refractive indexes. Bottom: relative and absolute differences between the extinction coefficients. All graphs use x=7.0, Number density (N) = 10^{12}

.

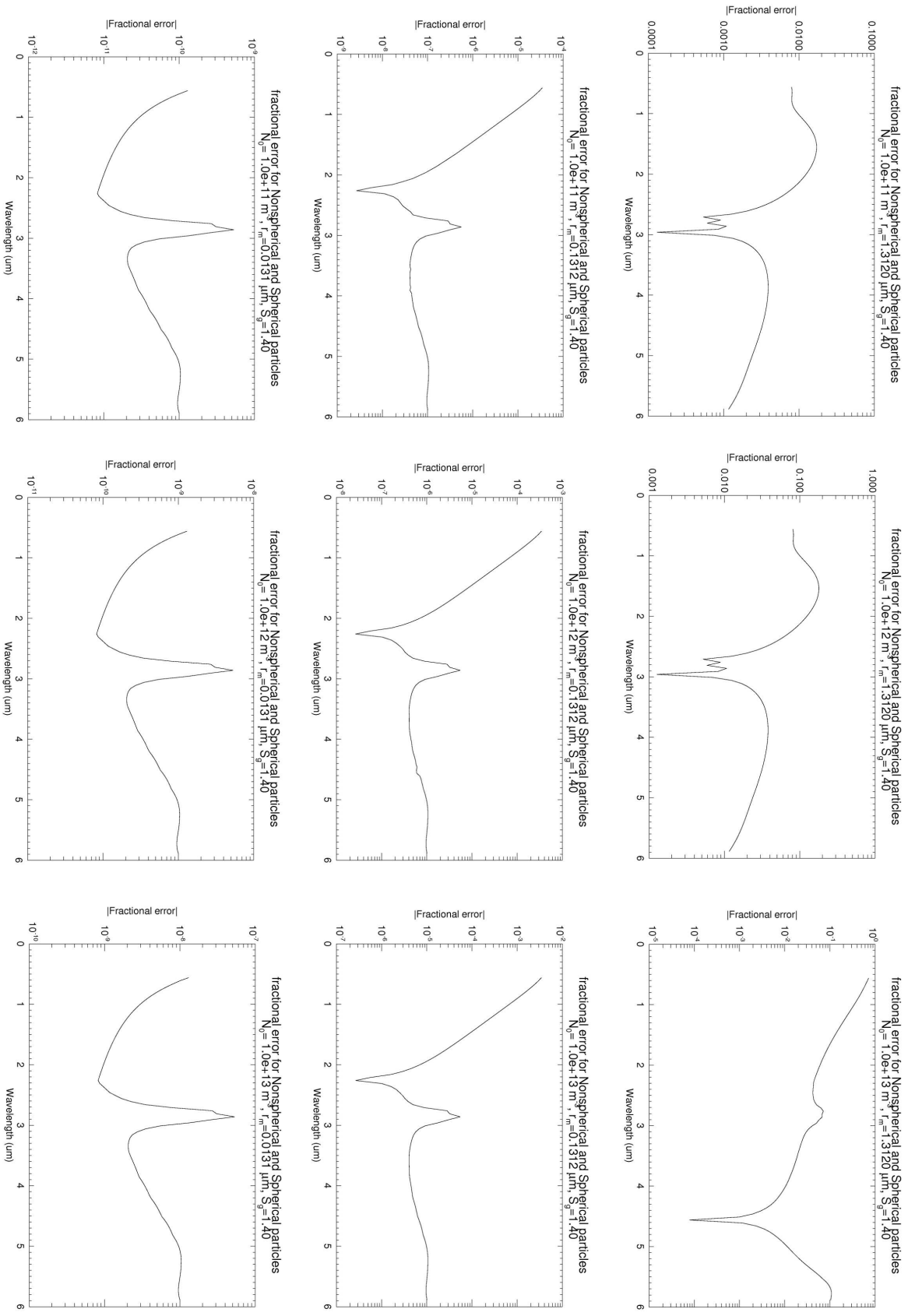

Figure 8: Plot of the fractional errors in transmittance between spherical and Non-spherical particles with an aspect ratio of 1.00 and 1.44 for a range of number densities and mean radii, using the Dubovik code and the flooring approximation.

Part II
Mie Maths

Introduction In order to calculate optical depth, it is necessary to calculate β^{ext}. This calculation involves solving a difficult integral, which is usually solved numerically, however, this method can be computationally expensive, and if the calculation needs to be repeated many times, it can become prohibitively so at resolutions large enough to encapsulate all of the fine structure of the integrand. As such, it is desirable to find numerical approximations to the integrand, which can be solved analytically, so that approximate results can be calculated at a much faster rate.

Useful Equations

$$\beta^{\text{ext}}(\lambda) = \int_0^\infty \pi r^2 Q^{\text{ext}}(\lambda, r) n(r)\, dr, \quad (1)$$

Here, $n(r)$ represents the number of particles with radii between r and $r + dr$. Aerosols tend to have a lognormal distribution of particles which can be given as

$$n(r) = \frac{1}{\sigma r \sqrt{2\pi}} \exp\left[-\frac{1}{2}\left(\frac{\ln r - \ln r_m}{\sigma}\right)^2\right] \quad (2)$$

where r_m is the mean radius and σ is the standard deviation of r for the distribution. Q^{ext} is a function calculated numerically from individual Mie calculations for each value of r. An example Q^{ext} can be seen in Figure 9.

Q^{ext} has several key features. For low values of x, the function grows rapidly from 0, and then decays to the value of 2 at large x. At a finer level, there is a regular oscillation, which can usually be encapsulated by the approximation. At the finest detail, there is an irregular oscillation usually termed the 'ripple structure'. This is the hardest part to calculate, as the finest elements of the ripple structure require a Δx of 10^{-6} to resolve. No further structure is revealed by decreasing Δx below 10^{-7}[3].

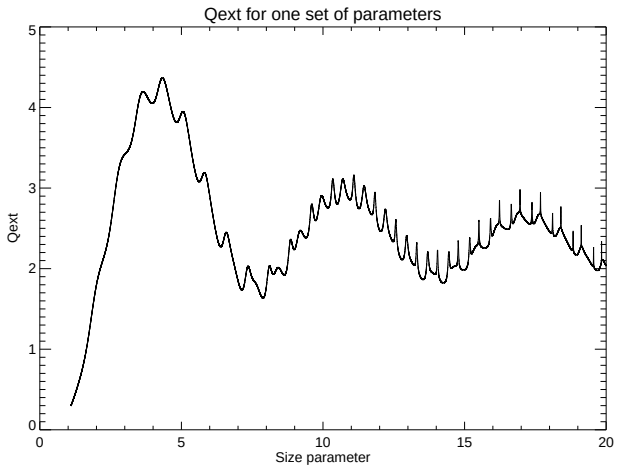

Figure 9: A typical Qext for a given set of parameters.

Previous work and how this work is different Several resources have already been published on ways to speed up the calculation[4][5]. A popular approach was to describe the entire integrand using several different formulas, each valid in different regimes, and then weighting them using the defining parameters to create a function that approximates the entire integrand. The downside of this approach is that the differences between the approximation and the exact integrand is fixed with respect to the defining parameters, and as such, when integrated, an upper limit on the accuracy of the approximation could be suggested, however this accuracy could not be increased.

The aim for this investigation was to create a program which, when given a required precision, would use analytical solutions to the upper and lower end of the integral, and calculate the intermediate range numerically. This approach then uses the least computational power necessary to provide the result at the required accuracy.

Lower limit At the low x limit, the Rayleigh approximation can be used. The derivation for both Q^{ext} and β^{ext} can be found in appendix A. To determine the largest possible x for a given target error, both the Rayleigh approximation and the actual values determined through Mie

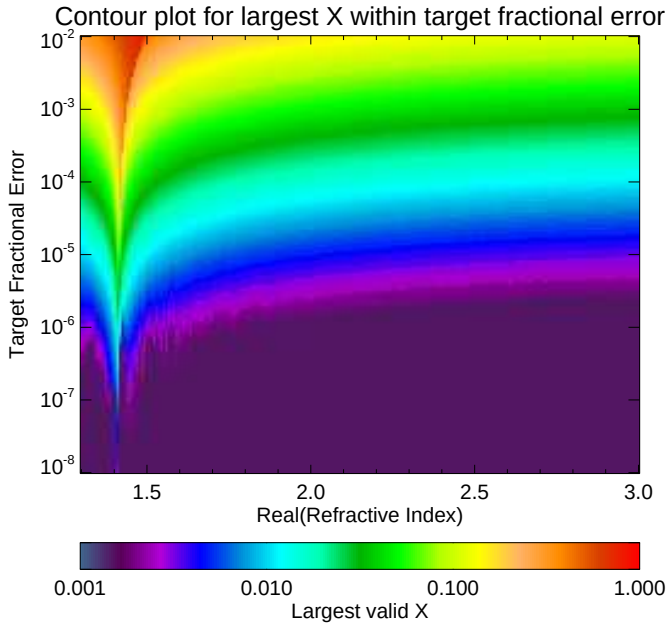

Figure 10: Plot of largest valid x for a given fractional error over a range of real refractive indexes.

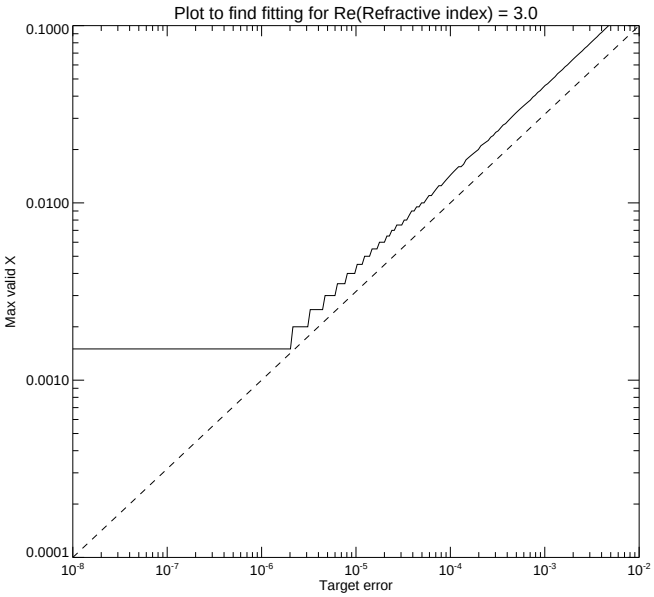

Figure 11: Plot of largest valid X for a given target fractional error. Solid line is from the calculation, dashed line is the $\sqrt{\text{target error}}$ approximation.

theory were calculated. A program was written to output the last value of x for which the approximation deviated from the Mie by less than the target error. The largest valid x was calculated over a range of target errors and real refractive indexes (the complex component was set to 0, as this results in the slowest decay of Q^{ext}, leading to the largest errors), and plotted in Figure 10.

It can be seen that, apart from around refractive index $\simeq 1.4$, refractive index has little effect on the largest valid x. As such, if a curve is fitted to the case where refractive index $= 3.0$, with no dependence on refractive index, it will give a largest valid x within the target error for any refractive index smaller than 3.

Largest valid x was plotted against target fractional error for this case, and it was observed that the line $x = \sqrt{\text{Target Fractional Error}}$ provided a relatively good fit (see Figure 11). As this is usually easy to compute, it was this formula that was used to calculate the maximum x for which the analytical solution for β^{ext} is valid.

In Figure 11, it can be seen that for target errors below about 10^{-6}, the largest valid x remains fixed. This is in fact an anomaly generated due to machine precision of the code used to calculate the Mie values of Q^{ext}. When plotting the error between the Rayleigh approximation and the calculated Mie values, the error should go to 0 as x goes to 0. Figure 12 shows that the error actually grows again as x decreases below the machine precision. As the Mie code was not designed for such small size parameters, the resolution of x in Figure 10 was limited, with the cutoff that appears in Figure 11 occuring at the first and smallest x used.

If the Rayleigh approximation is taken to be correct at the low x limit, then the $\sqrt{\text{error}}$ would remain a suitable approximation, as the fitted line extrapolates to 0, which makes physical sense. This would be a difficult hypothesis to verify, as it would require rewriting the Mie code for a higher precission.

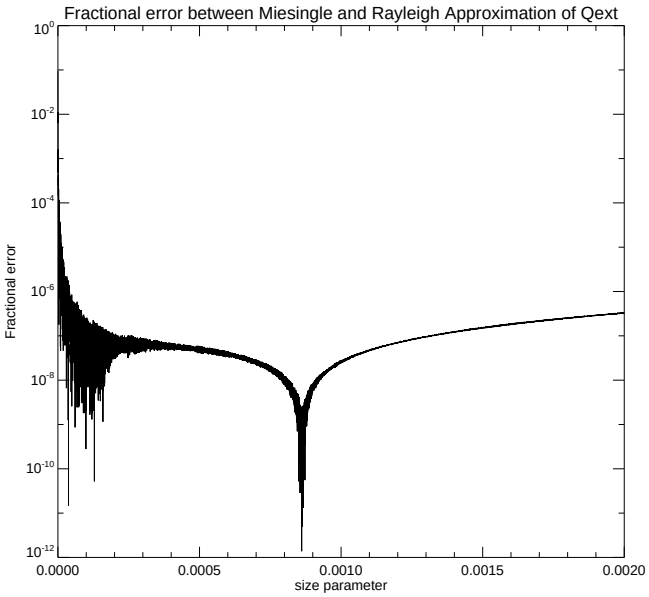

Figure 12: Fractional error between Mie calculation and the Rayleigh approximation in the regime where the Mie code exceeds machine precision. The spike corresponds to the error changing signs.

Upper limit

Real m At the upper end of the integral, equation 3 [5]can be used to replace Q^{ext} in the β^{ext} integral.

$$Q^{\text{ext}}_{1^{st}approx} = 2 + 1.9923861x^{-2/3} + \frac{2}{x}\,\text{Im}\left\{\frac{(m^2+1)}{(m^2-1)^{1/2}}\right\} - 0.7153537x^{-4/3} \quad (3)$$

As the ripple structure has very narrow, but large peaks for certain values of m, it is difficult to determine the value of x for which these peaks generate errors less than the target error. To find this smallest valid x, an envelope function for the ripple function is required. Once a smallest valid x has been determined, it can be used in the analytical solution derived in appendix B. It was observed that the largest deviation from the approximation in equation 3 occurred around the peak values of the periodic oscillation in Q^{ext}, with the Mie calculation always greater than the approximation. Using equations from van de Hulst ($\sim$ p179)[4], it was calculated that Q^{ext} has maxima peaks at values of

$$x_n = \left[\frac{3\pi}{2} - \arctan\left(\frac{b}{a-1}\right) + 2\pi n\right]/2(a-1)$$

where $m = a + ib$, and $n \geq 0$. As these values are dependent on m, the x values used need to be recalculated for each refractive index of interest. When looking over a range of x's, the closest peak value x_n to the x provided by whichever quadrature used was used for each given m.

A programme was written to look at x values within a range of 10^{-4} either side of a given peak x at a resolution of 10^{-6}. The x that provided the largest error, and the corresponding fractional error were recorded over a range of x's and m's. These were plotted in Figure 13. This plot shows that the real component

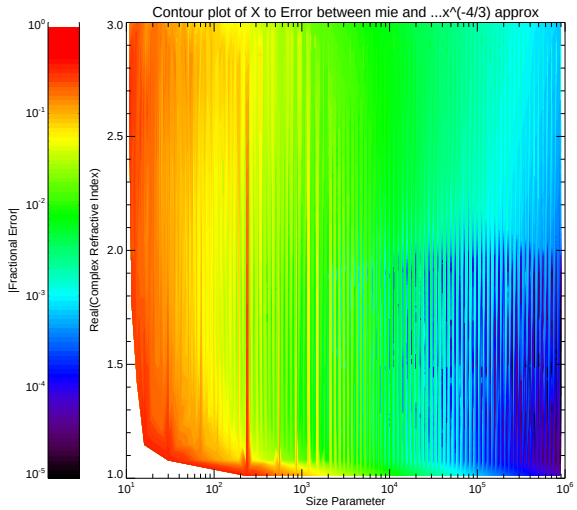

Figure 13: Contour plot of the maximum |Fractional error| between the approximation in equation 3 and the Mie calculation over a range of x's and m's.

above a certain point has little effect on the x to error curves. To calculate the lowest valid x using this plot, the worst case fit should again be used, but as the range of interest is really between 1.3 $\leq$Re(m)$\leq$ 1.6, we can isolate appropriate worst fits for each region of the m, for example by subdividing the refractive indexes

into four regimes, 1 to 1.1, 1.1 to 1.3, 1.3 to 1.6, and 1.6 to 3.0. The plots for Re(m)= 1.6, Re(m)= 3.0, Re(m)= 1.1 and Re(m)= 1.01 can be seen in Figures 14,15,16 and 17 respectively. The best fit equations are provided in the figures' captions.

These equations can now be used to calculate the lowest valid x for a given Re(m) and a target error.

Complex m So far, only the real component of m has been investigated. To investigate the effect of a complex m, the fractional error between the approximation in equation 3 and the Mie calculation was plotted over a range of imaginary components of m and x's, with a fixed real part. The plot for Re(m) = 1.5 can be seen in Figure 18.

The dark blue 'valley' is due to the error changing sign as it passes through zero, and for different values of Re(m), the value of Im(m) at which this occurs varies. An approximation was derived to try and model this error, so as to enable a better approximation of Q^{ext}. The plot of this approximate error can be seen in Figure 19. The equation for this plot is given by equation 4.

$$\text{Fractional Error Approx} = -1.907987457x^{\frac{-1.4}{\ln 4}}(b - \sqrt{1 - 0.64(a - 0.5)^2}) \quad (4)$$
$$\text{for} 1 < a \leqslant 1.75$$

$$Q^{\text{ext}}_{2^{nd}approx} = \frac{Q^{\text{ext}}_{1^{st}approx}}{1 + \text{Fractional Error Approx}} \quad (5)$$

These two plots look similar in certain regimes. By removing the approximate error from $Q^{\text{ext}}_{1^{st}approx}$, a better fit for the Q^{ext} can be obtained. The equation for this new approximation can be seen in equation 5. Unfortunately this is still rather inaccurate, but it is a slightly better approximation in many regimes, especially those with large Im(m)'s, and is recorded here as all papers read by the author on the topic only covered Im(m) < 0.01. If a suitably accurate approximation was to be found, it could be used in place of the Mie calculation to speed up the computation of the numerical integral.

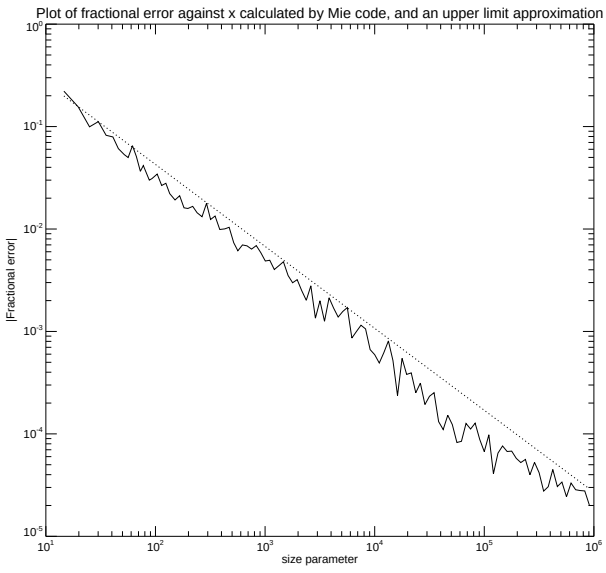

Figure 14: Plot of |Fractional Error| against x for Re(m) = 1.6. The Solid line is the Max values from the Mie calculation, and the dotted line is the approximation $|\text{error}| = 1.7x^{-0.8}$

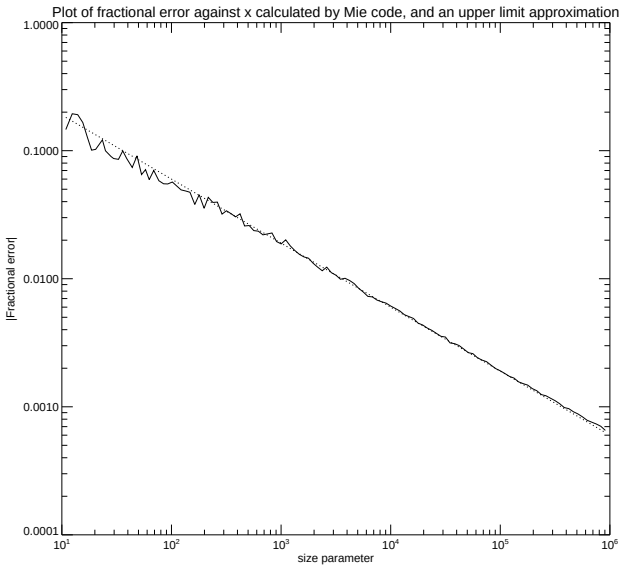

Figure 15: Plot of |Fractional Error| against x for Re(m) = 3.0. The Solid line is the Max values from the Mie calculation, and the dotted line is the approximation $|\text{error}| = 0.6x^{-0.5}$

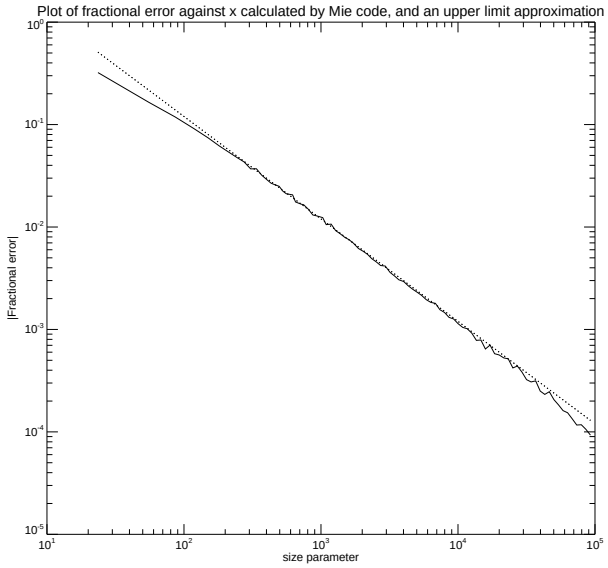

Figure 16: Plot of |Fractional Error| against x for $\mathrm{Re}(m) = 1.1$. The Solid line is the Max values from the Mie calculation, and the dotted line is the approximation $|\text{error}| = 12x^{-1}$

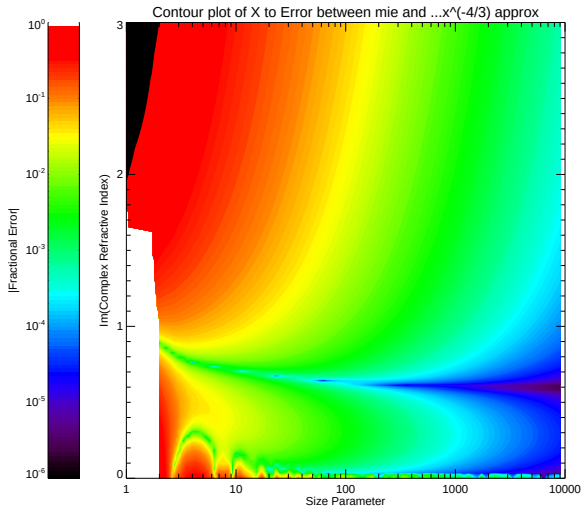

Figure 18: Contour plot of error between equation 3 and the Mie calculation for $\mathrm{Re}(m) = 1.5$.

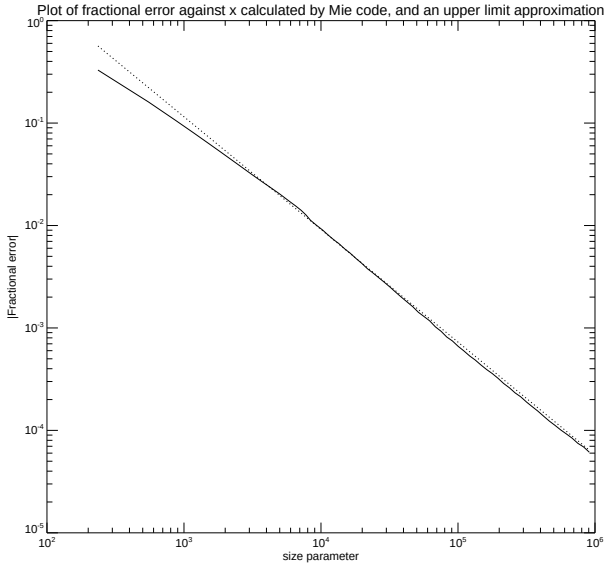

Figure 17: Plot of |Fractional Error| against x for $\mathrm{Re}(m) = 1.01$. The Solid line is the Max values from the Mie calculation, and the dotted line is the approximation $|\text{error}| = 230x^{-1.1}$

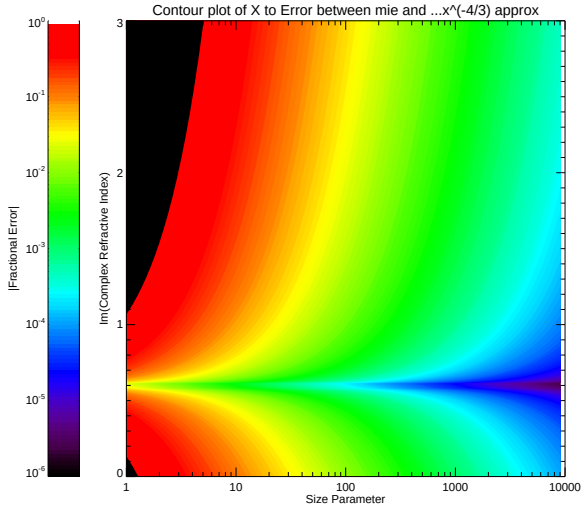

Figure 19: Contour plot of an approximation to the error between equation 3 and the Mie calculation for $\mathrm{Re}(m) = 1.5$. The approximation used can be seen in equation 4.

Figure 18 is useful as it shows certain regimes. For Im(m)$\lesssim$ 0.01, larger errors persist to much larger values of x. In this regime, the approach used for Im(m)= 0 can be used, as the ripple structure remains visible, only with a smaller amplitude.

For 0.01 $\lesssim$<Im(m)$\lesssim$ 0.05, the ripple structure becomes much less significant, but the sinusoidal oscillation remains prominent, however it does decay rapidly. This can be seen in Figure 18 as large, patterned errors for $x \lesssim$ 100, and then very small errors for larger x's. Due to the negligibility of the ripple structure, only one value of x at each peak of the oscillation (x_n) needs to be calculated to determine above which x $Q^{\text{ext}}_{1^{st}approx}$ remains within the target error. As Q^{ext} converges to $Q^{\text{ext}}_{1^{st}approx}$, this value can then be used as the lowest valid x in the analytical solution (appendix B).

For 0.05 $\lesssim$Im(m), only a few (if any) oscillations remain before Q^{ext} becomes a smooth, decaying function. Unfortunately, this function can no longer be approximated by $Q^{\text{ext}}_{1^{st}approx}$, as they do not converge until very large x's. The time saving solution in this regime would be to use numerical integration, but with a very sparse quadrature. As only a few points would be necessary in the calculation, computational time could be greatly reduced. If the x values used corresponded to the zero's of the sinusoidal oscillation, then any remaining (very small) parts of the oscillation would be averaged out correctly.

The first peak of Q^{ext} falls into the 'middle' section of the integral, as it does not fit to either the upper or lower end approximation. As this peak also affects the behaviour of the function at x's close to it, a good rule of thumb would be to always use numerical integration to solve the region $x_{largestvalid} < x \lesssim 50$. For $x \gtrsim 50$, Q^{ext} has usually converged to the relevant approximation and the aforementioned solutions can be used.

Conclusions The integral for β^{ext} can be calculated to within a target error by approximating Q^{ext} differently in different regimes. In the low x regime, the analytical solution in appendix A can be used where the largest valid x is given by $\sqrt{\text{target error}}$. In the high x limit, the approximation used depends on the real and imaginary components of m. For Im(m)$\lesssim$ 0.01, the analytical solution in appendix B can be used, calculating the lowest valid x (x_l) with the below formulas, depending on Re(m).

- For 1.0 <Re(m) $\leq$ 1.1,
  $x_l = (\text{target error}/230)^{-\frac{10}{11}}$
- For 1.1 < Re(m) $\leq$ 1.3,
  $x_l = (\text{target error}/12)^{-1}$
- For 1.3 <Re(m) $\leq$ 1.6,
  $x_l = (\text{target error}/1.7)^{-\frac{5}{4}}$
- For 1.6 <Re(m),
  $x_l = (\text{target error}/0.6)^{-2}$

For 0.01 $\lesssim$Im(m)$\lesssim$ 0.05, the Mie calculation must be completed at increasing x_n's until the fractional error between the Mie Q^{ext} and the approximate $Q^{\text{ext}}_{1^{st}approx}$ is less than the target error. After this, the integral can be calculated analytically using appendix B. For 0.05 $\lesssim$Im(m), there is not yet an analytical solution, and the integral must be calculated numerically, however, as there is little to no oscillating structure beyond about $x = 50$, a sparse quadrature can be used. Also, if instead of peak values x_n being used as the quadrature points, using $x_{n+0.25}$, the zeros of the oscillation, would result in any oscillations being averaged out.

For all values of m, it is recommended that care should be taken when using upper end approximations with $x \lesssim 50$, as this region has not yet been sufficiently investigated, and in some situations, the approximations and Q^{ext} have not yet converged.

Future work The most obvious future work is to look at the middle section of the integral. As this range could greatly change in size as parameters are altered, deducing the necessary quadrature for the given range would

allow faster computation for specified accuracies, without doing unnecessary work. A second possible development would be finding a good approximation for Q^{ext} for larger $\text{Im}(m)$, as none seem to yet exist. This could then be used to calculate more points in the numerical integral as the calculation should take less time than a full Mie computation. A third possible investigation would be into the behaviour of the Mie code at very small x's, as seen in Figure 12.

References

[1] *Dan's Aso Ash Data*, Daniel Peters

[2] *Dubovik_lognormal program*, Andrew Smith

[3] Chýlek et al. (1978a)

[4] *Light Scattering by Small Particles*, H.C. van de Hulst,(1957)

[5] *Simple approximation to extinction efficiency valid over all size parameters*, Evans and Fournier, Applied Optics Vol. 29, No. 31, 1st November 1990

A Analytical Solution to Lower limit

The Rayleigh approximation for small x can be written as

$$Q^{\text{ext}}(x,m) \simeq 4x \,\text{Im}\left\{\frac{m^2-1}{m^2+2}\left[1+\frac{x^2}{15}\left(\frac{m^2-1}{m^2+2}\right)\frac{m^4+27m^2+38}{2m^2+3}\right]\right\} + \frac{8}{3}x^4 \,\text{Re}\left\{\left(\frac{m^2-1}{m^2+2}\right)^2\right\}$$

Where $x = \frac{2\pi r}{\lambda}$, the size parameter, and $m = a + ib$ is the complex relative refractive index. Expanding each of the parts of the imaginary section in turn gives:

$$\frac{m^2-1}{m^2+2} = 1 - \frac{3}{2+(a+ib)^2} = \frac{a^4+b^4+a^2-b^2+2a^2b^2-2+6iab}{4a^2b^2+(a^2-b^2+2)^2} = \alpha + i\beta \tag{6}$$

$$\frac{m^4+27m^2+38}{2m^2+3} = \frac{i(4a^5b+12a^3b+8a^3b^3+10ab-12ab^3+4ab^5)}{16a^2b^2+(2(a^2-b^2)+3)^2} + \frac{2a^6-2b^6-2a^2b^4+57a^4+57b^4+2a^4b^2+90a^2b^2+157a^2-157b^2+114}{16a^2b^2+(2(a^2-b^2)+3)^2} = i\chi + \rho \tag{7}$$

which gives

$$\begin{aligned} Q^{\text{ext}}(x,m) &= 4x \,\text{Im}\left\{(\alpha+i\beta)\left(1+\frac{x^2}{15}(\alpha+i\beta)(\rho+i\chi)\right)\right\} + \frac{8}{3}x^4 \,\text{Re}\left\{(\alpha+i\beta)^2\right\} \\ &= \frac{4}{15}x^3[\alpha(\alpha\chi+\beta\rho)+\beta(\alpha\rho-\beta\chi)] + 4x\beta + \frac{8}{3}x^4(\alpha^2-\beta^2) \end{aligned}$$

Substituting $x = \frac{2\pi r}{\lambda}$ and rearranging gives:

$$\begin{aligned} Q^{\text{ext}}(x,m) &= \frac{8}{3}(\alpha^2-\beta^2)\left(\frac{2\pi}{\lambda}\right)^4 r^4 + \frac{4}{15}[(\alpha^2-\beta^2)\chi + 2\beta\alpha\rho]\left(\frac{2\pi}{\lambda}\right)^3 r^3 + 4\beta\left(\frac{2\pi}{\lambda}\right) r \\ &= \zeta r^4 + \xi r^3 + \eta r \end{aligned}$$

Using the log-normal distribution, and the above result,

$$\beta^{\text{ext}}(\lambda) = \frac{N_0}{\ln S}\sqrt{\frac{\pi}{2}}\int_0^\infty r(\zeta r^4 + \xi r^3 + \eta r)\exp\left[-\frac{1}{2}\left(\frac{\ln r - \ln r_{\text{m}}}{\ln S}\right)^2\right] dr$$

Applying the substitutions:

$$\begin{aligned} t &= \frac{\ln r - \ln r_{\text{m}}}{\ln S}, \qquad t(0) = -\infty, \qquad t(\infty) = \infty \\ r &= e^{t\ln S + \ln r_{\text{m}}} \\ \frac{dr}{dt} &= \ln S e^{t\ln S + \ln r_{\text{m}}} = r\ln S \end{aligned}$$

$$\beta^{\text{ext}}(\lambda) \;=\; N_0\sqrt{\frac{\pi}{2}}\int_{-\infty}^{\infty}(\zeta r^6+\xi r^5+\eta r^3)\exp\left[-\frac{1}{2}t^2\right]\,dt$$

Solving this in general for each r^n component:

$$\begin{aligned}&\int_{-\infty}^{\infty} r^n\exp\left[-\frac{1}{2}t^2\right]\,dt\\ =&\int_{-\infty}^{\infty}\exp\left(nt\ln S+n\ln r_{\text{m}}\right)\exp\left[-\frac{1}{2}t^2\right]\,dt\\ =\;& r_{\text{m}}^n\int_{-\infty}^{\infty}\exp\left[-\frac{1}{2}t^2+nt\ln S\right]\,dt\end{aligned}$$

Use the definition:

$$\int_a^{\infty} e^{-q^2x^2-px}\,dx \;=\; \frac{\sqrt{\pi}}{2q}e^{p^2/4q^2}\left[1-\text{erf}\left(\frac{p+2aq^2}{2q}\right)\right]$$

Change of variable to in $y=-x$ gives

$$\int_{-a}^{-\infty}-e^{-q^2y^2+py}\,dy=\int_{-\infty}^{-a}e^{-q^2y^2+py}\,dy \;=\; \frac{\sqrt{\pi}}{2q}e^{p^2/4q^2}\left[1-\text{erf}\left(\frac{p+2aq^2}{2q}\right)\right]$$

Hence

$$\int_{-\infty}^{-t_l}\exp\left[-\frac{1}{2}t^2+nt\ln S\right]\,dt \;=\; \frac{\sqrt{\pi}}{\sqrt{2}}e^{\frac{n^2}{2}\ln^2 S}\left[1-\text{erf}\left(\frac{n\ln S+t_l}{\sqrt{2}}\right)\right]$$

Which gives the lower limit β^{ext}:

$$\begin{aligned}\beta^{\text{ext}}=N_0\frac{\pi}{2}\Bigg\{&e^{\frac{36}{2}\ln^2 S}\left[1-\text{erf}\left(\frac{6\ln S+t_l}{\sqrt{2}}\right)\right]r_{\text{m}}^6\zeta\\ &+e^{\frac{25}{2}\ln^2 S}\left[1-\text{erf}\left(\frac{5\ln S+t_l}{\sqrt{2}}\right)\right]r_{\text{m}}^5\xi\\ &+e^{\frac{9}{2}\ln^2 S}\left[1-\text{erf}\left(\frac{3\ln S+t_l}{\sqrt{2}}\right)\right]r_{\text{m}}^3\eta\Bigg\}\end{aligned}$$

B Analytical Solution to Upper limit

Above a certain value of x, the fine structure of Q^{ext} can be approximated by the function [5]

$$Q^{\text{ext}} = 2 + 1.9923861x^{-2/3} + \frac{2}{x}\,\text{Im}\left\{\frac{(m^2+1)}{(m^2-1)^{1/2}}\right\} - 0.7153537x^{-4/3} \tag{8}$$

Again using $x = \frac{2\pi r}{\lambda}$ and collecting the coefficients for each power of r, the

$$\beta^{\text{ext}}(\lambda) \;=\; \frac{N_0}{\ln S}\sqrt{\frac{\pi}{2}}\int_0^\infty r(2 + \mu r^{-2/3} + \nu r^{-1} + \kappa r^{-4/3})\exp\left[-\frac{1}{2}\left(\frac{\ln r - \ln r_{\text{m}}}{\ln S}\right)^2\right] dr$$

where

$$\mu = 1.9923861\left(\frac{2\pi}{\lambda}\right)^{-2/3}$$
$$\nu = 2\,\text{Im}\left\{\frac{(m^2+1)}{(m^2-1)^{1/2}}\right\}\left(\frac{2\pi}{\lambda}\right)^{-1}$$
$$\kappa = -0.7153537\left(\frac{2\pi}{\lambda}\right)^{-4/3}$$

Applying the same substitutions before, the equations can be written as

$$\beta^{\text{ext}}(\lambda) \;=\; N_0\sqrt{\frac{\pi}{2}}\int_{-\infty}^\infty (2r^2 + \mu r^{4/3} + \nu r + \kappa r^{2/3})\exp\left[-\frac{1}{2}t^2\right] dt$$

Using the formula derived above

$$\int_{-\infty}^\infty r^n \exp\left[-\frac{1}{2}t^2\right] dt = r_{\text{m}}^n \int_{-\infty}^\infty \exp\left[-\frac{1}{2}t^2 + nt\ln S\right] dt$$

and the definition

$$\int_a^\infty e^{-q^2x^2 - px}\,dx \;=\; \frac{\sqrt{\pi}}{2q}e^{p^2/4q^2}\left[1 - \text{erf}\left(\frac{p + 2aq^2}{2q}\right)\right]$$

gives the upper limit integral to be

$$\beta^{\rm ext} = N_0 \frac{\pi}{2} \left\{ e^{\frac{8}{9}\ln^2 S} \left[1 - {\rm erf}\left(\frac{-\frac{4}{3}\ln S + t_u}{\sqrt{2}} \right) \right] r_{\rm m}^{4/3} \mu \right.$$
$$+ e^{\frac{1}{2}\ln^2 S} \left[1 - {\rm erf}\left(\frac{-\ln S + t_u}{\sqrt{2}} \right) \right] r_{\rm m} \nu$$
$$+ e^{\frac{2}{9}\ln^2 S} \left[1 - {\rm erf}\left(\frac{-\frac{2}{3}\ln S + t_u}{\sqrt{2}} \right) \right] r_{\rm m}^{2/3} \kappa$$
$$\left. + 2e^{2\ln^2 S} \left[1 - {\rm erf}\left(\frac{-2\ln S + t_u}{\sqrt{2}} \right) \right] r_{\rm m}^2 \right\}$$

C General case for $Q^{\rm ext} = ax^n$

If $Q^{\rm ext} = ax^n$, then for the lower end,

$$\beta^{\rm ext} = aN_0 \frac{\pi}{2} e^{\frac{(n+2)^2}{2}\ln^2 S} \left[1 - {\rm erf}\left(\frac{({\rm n}+2)\ln {\rm S} + {\rm t_l}}{\sqrt{2}} \right) \right] r_{\rm m}^{n+2} \left(\frac{2\pi}{\lambda} \right)^n$$

and for the upper end

$$\beta^{\rm ext} = aN_0 \frac{\pi}{2} e^{\frac{(n+2)^2}{2}\ln^2 S} \left[1 - {\rm erf}\left(\frac{-({\rm n}+2)\ln {\rm S} + {\rm t_u}}{\sqrt{2}} \right) \right] r_{\rm m}^{n+2} \left(\frac{2\pi}{\lambda} \right)^n$$

Multiple powers of x can be used in $Q^{\rm ext}$ by adding the above solutions with different ns. Caution must be taken when defining t_l as the solution is for the integral from $-\infty$ to $-t_l$. It is also useful to use the erfc (complimentary error function) if IDL is being used, as this works for lower values of t_l.